Title: Rapid progression is associated with lymphoid follicle dysfunction in SIV-infected infant rhesus macaques

Short Title: Lymphoid Dysfunction and Rapid SIV Progression in Infant Macaques

Matthew P. Wood[1], Chloe I. Jones[1], Adriana Lippy[1], Brian G. Oliver[1], Brynn Walund[1], Katherine A. Fancher[1], Bridget S. Fisher[1], Piper J. Wright[1], James T. Fuller[2], Patience Murapa[2,3], Jakob Habib[4,5], Maud Mavigner[4,5], Ann Chahroudi[4,5], D. Noah Sather[1], Deborah H. Fuller[2,3], Donald L. Sodora[1]

1 Center for Global Infectious Disease Research, Seattle Children's Research Institute, Seattle, Washington, USA

2 University of Washington Department of Microbiology, Seattle, WA

3 Washington National Primate Research Center, Seattle WA

4 Yerkes National Primate Research Center, Emory University School of Medicine, Atlanta, Georgia, USA

5 Department of Pediatrics, Emory University School of Medicine, Atlanta, Georgia, USA

6 Center for Childhood Infections and Vaccines of Children's Healthcare of Atlanta and Emory University, Atlanta, GA USA

Abstract

HIV-infected infants are at an increased risk of progressing rapidly to AIDS in the first weeks of life. Here, we evaluated immunological and virological parameters in 25 SIV-infected infant rhesus macaques to understand the factors influencing a rapid disease outcome. Infant

macaques were infected with SIVmac251 and monitored for 10 to 17 weeks post-infection. SIV-infected infants were divided into either typical (TypP) or rapid (RP) progressor groups based on levels of plasma anti-SIV antibody levels and SIV plasma viral load (with RP infants having low SIV-specific antibodies and high viral loads). Following SIV infection, 11 out of 25 infant macaques exhibited an RP phenotype, with 5 of these succumbing to AIDS-related infections. Interestingly, the TypP and RP infants were similar in their CD4 depletion and activation of CD8 T cells as measured by the levels of HLA-DR on the cell surface. However, differences between the two groups were identified in other immune cell populations, including a failure to expand activated memory (CD21-CD27+) B cells in peripheral blood in RP infant macaques, as well as reduced levels of germinal center (GC) B cells and T follicular helper (Tfh) cells in spleens (4- and 10-weeks post-SIV). Reduced B cell proliferation in splenic germinal GCs was associated with increased SIV+ cell density and follicular type 1 interferon (IFN)-induced immune activation. Further analyses determined that at 2-weeks post SIV infection TypP infants exhibited elevated levels of the GC-inducing chemokine CXCL13 in plasma, as well as significantly lower levels of viral envelope diversity compared to RP infants. Our findings provide evidence that early viral and immunologic events following SIV infection contributes to impairment of B cells, Tfh cells and germinal center formation, ultimately impeding the development of SIV-specific antibody responses in rapidly progressing infant macaques.

Key words: HIV, SIV, Infants, B cells, Spleen, oral transmission

Introduction

Despite significant reductions in vertical HIV transmission, nearly 100,000 children succumb to AIDS-related illnesses each year (1). This can be in part attributed to a

53 disproportionately higher risk of progressing to AIDS, with roughly half of infected infants
54 exhibiting rapid disease progression within the first two years of life (2-7). Despite this
55 observation being first reported early in the epidemic (4, 8), factors influencing why some infants
56 exhibit a rapid HIV progression phenotype have yet to be fully understood.

57 Acute HIV infection is characterized by exponential viral replication in blood and tissues,
58 depletion of mucosal CD4 T cells, production of type 1 interferons (IFNs) and increased IFN-
59 induced gene transcription (9). This is typically followed by an expansion of activated B cells in
60 the blood and lymph nodes and production of anti-HIV antibodies targeting viral envelope
61 proteins (10). While the initial reduction of viral replication coincides with antibody production,
62 antibodies produced during this period lack virus neutralizing activity, and viral control at the
63 onset of chronic infection is often attributed to CD8 T cell responses (11, 12). However, in
64 infants and children who progress rapidly to AIDS, plasma viral loads remain elevated well
65 beyond acute infection, resulting in sustained type 1 IFN production (13), increased levels of
66 inflammatory immune mediators (14, 15) and a failure to develop humoral HIV responses (4).

67 Much of our mechanistic understanding of rapid progression to AIDS in infants comes
68 from the macaque SIV model (16-18). Previous studies demonstrated that a proportion of infant
69 macaques infected through repeated oral exposures generally exhibited several characteristics
70 consistent with rapid HIV infection in infant humans; including high plasma viral loads following
71 acute infection and an absence of virus-specific plasma antibodies (19, 20). Other studies
72 demonstrated that SIV infects, and presumably replicates within, multiple oral mucosal and
73 associated lymphoid tissues by as early as 24 hours, before spreading to several distal tissue
74 sites (18, 21). Macaques that fail to reduce viral load following acute infection also have been
75 shown to exhibit elevated and sustained type 1 IFN-induced gene expression in lymphoid
76 organs (22, 23).

77 Given that lymphoid tissues are critical for B cell development within germinal centers,
78 and that macaques that rapidly progress to AIDS fail to develop humoral responses (24-27), we

hypothesized that early viral replication and associated aberrant innate activation impairs B cell follicle function and prevents initial humoral responses following acute SIV infection. Here we have assessed samples from 25 infant rhesus macaques, 11 of which failed to produce substantial plasma concentrations of anti-SIV antibodies and exhibiting a phenotype consistent with rapid progression (RP). In contrast, 14 infant macaques exhibited a more typical disease progression phenotype (TypP), similar to that observed in adult animals. However, RP infants were distinct in that they possessed higher SIV genetic diversity in blood during acute infection, and did not increase plasma CXCL13 following infection. In addition, they exhibited significantly elevated plasmacytoid dendritic cell (pDC) activation and increased type I IFN mediated protein expression in B cell follicles, as well as dramatically elevated IFNα levels in blood during chronic infection. These results support a model wherein early events following infection drive aberrant innate responses, which are associated with lymphoid dysfunction and failure to develop humoral immunity in rapidly progressing HIV/SIV-infected infants.

Results

Oral SIV infection in macaque infants results in similar proportions of infants with rapid and typical disease progression. To evaluate the pathogenic outcome following oral mucosal SIV infection, infant rhesus macaques were infected through a series of escalating dose oral challenges with SIVmac251 and monitored for up to 22 weeks (median 10 weeks)(**Fig. 1A**). SIV plasma viral load was measured throughout the time course (**Fig. 1B**), and we focused on time points that reflect acute (2 weeks post-SIV), acute-chronic transition (4-6 weeks post-SIV) and the chronic phase (10+ weeks) of infection to assess differences over time. (**Fig. 1C**). Plasma levels of anti-gp130 (Env)-specific IgG (**Fig. 1D**) and IgA **(Fig. 1E**) antibodies were evaluated at weeks 0, 4-6, and 10-12 post-SIV. Based on these observations, SIV-infected infant macaques can be divided into rapid progressors (RP) being those with the highest viral loads after week 2 and undetectable or very low levels of SIV-Env specific IgG and IgA antibodies during chronic

105 infection. Factors that were not associated with rapid disease progression included SIV dose,
106 sex or previous vaccination from a separate study (**Table 1**). Age also did not appear to be a
107 factor contributing to disease progression, with median ages of SIV acquisition for TypP and RP
108 macaques being 11 weeks and 13 weeks, respectively. Additionally, 8 of 11 RP macaques
109 developed clinical signs of simian AIDS prior to the end of the study follow-up, based on reports
110 from veterinary staff. All infants showing clinical signs of AIDS exhibited either chronic SIV-
111 associated diarrheal disease, failure to gain weight and wasting. This finding is consistent with
112 earlier reports of SIV pathology in rapidly progressing macaques, with severe enteropathy and
113 wasting observed in the absence of opportunistic infections (28).
114
115 **Acute stage levels of unique plasma viral variants negatively correlate with chronic stage**
116 **anti-SIV antibodies.** Based on previous work linking viral genetic diversity at acute infection
117 with disease outcome (29), we evaluated viral diversity by the number of V1V2 Env variants
118 during acute infection. Plasma was obtained at 2 weeks post-SIV infection and viral diversity
119 within V1V2 region of SIV envelope assessed by Illumina miSeq. This V1V2 478 bp region was
120 selected as it contained the highest degree of DNA sequence variability within our SIVmac251
121 challenge strain. Representative phylogenies constructed by maximum likelihood are depicted
122 for TypP (**Fig. 2A**) and RP (**Fig. 2B**) infants. After enumerating unique variant clusters in each
123 infant group, we observed a significantly greater number of variants present at 2 weeks post-
124 SIV in the RP compared to TypP macaques (**Fig. 2C**). We also observed an inverse correlation
125 between the anti-SIV-ENV IgG level (at week 10-12) and the number of observed V1V2 variant
126 clusters (**Fig. 2D**). Phylogenetic assessment of V1V2 variants in the SIVmac251 challenge
127 stock and infant macaque plasma revealed that variants from RP infants are represented across
128 a greater number of clades sharing sequences with the challenge stock than those from TypP
129 infants (**Fig. S1A and S1B**), indicating a more diverse genetic background in RP infant-derived
130 plasma SIV. Greater genetic diversity in V1V2 of RP infant macaques suggests that RP infants

are either infected with a greater number of SIV founders originating from the challenge stock, or that when macaques are initially infected, there are increased levels of SIV replication, and consequently accumulated mutations, within RP infants at 2 weeks post-SIV infection compared to the TypP infants.

Total CD4 T cell levels are sustained during chronic infection of RP infants. To assess CD4 T cell depletion in SIV-infected infants, numbers of CD4 and CD8 T cells per mL of whole blood were used to calculate the CD4/CD8 ratio over time. Surprisingly, similar CD4/CD8 ratios were observed in both groups of infants at each time point examined (**Fig. 3A and 3B**). Assessment of total CD4+ T cells (CD4+, CD3+) in peripheral blood revealed that RP infants had similar levels of CD4 cells pre-SIV infection through early chronic infection, compared to TypP infants. However, CD4 levels were significantly higher in the RP group (mean 3.2 fold increase) during chronic infection (**Fig. 3C**). This increased CD4 levels in RP macaques potentially reflects an expansion of naive T cells, which has previously been reported (28). This finding indicates that the infant RP phenotype is not associated with depletion of total peripheral CD4 T cells.

Chronic activation of CD4 and CD8 T cells is an established correlate of progression to AIDS in both HIV and SIV infections (30-32). To explore the link between T cell activation and the rapid progression phenotype observed in infant macaques, the levels of HLA-DR were assessed on T cell subsets within both macaque groups (**Fig. 4A, B**). The level of HLA-DR+ CD8 T cells was significantly increased in the TypP at both 4-6 (2.9-fold) and 10-12 (6.6-fold) weeks post-SIV (**Fig. 4A**). In the CD4+ population, the TypP macaques exhibited modest yet significant increases in HLA-DR levels at the 4-6 week time point (1.7-fold) (**Fig. 4B**). Loss of gut barrier function and associated microbial translocation has been characterized as a significant driver of T cell activation and inflammation during both chronic HIV and SIV infections (31, 33). To evaluate microbial translocation in TypP and RP infants, soluble CD14 (sCD14) and

LPS binding protein (LPB) concentrations were measured in plasma collected at weeks 0, 2, 4-6, and 10-12 post-SIV (**Figure S2A, B**). These findings demonstrate that despite a more rapid disease progression, the RP infants exhibit similar levels of sCD14 and LPB, as well as unexpectedly low levels of CD4 and CD8 T cell activation.

Rapidly progressing infants fail to increase activated memory B cells during chronic infection. The lack of SIV-specific antibodies in the RP infant macaques raised the question as to whether memory B cell levels and activation were altered in RP compared to the TypP macaques. Assessment of B cells levels within peripheral blood revealed that the percentage of B cells (%CD20+ of CD3- PBMCs) was 1.5-fold higher at 10 to 12 weeks post-SIV in the TypP macaques compared to RP (**Fig. 5A**). Bidirectional interactions between T cells and B cells are necessary for effective humoral responses, and ineffective B cell costimulatory function has previously been linked to impaired CD80 expression on B cells of HIV-viremic patients (34). Comparing CD80+ B cells in RP and TypP macaques revealed that RP infants failed to increase the levels of this cell population during early chronic infection (**Fig. 5B**). By 5 weeks post-SIV TypP infants exhibited significantly higher CD80+ B cells than RP infants and this trend continued through 12 weeks post-infection, with TypP infants having on average 8.4-fold higher levels of circulating B cells expressing CD80. To further characterize changes in B cell populations following infection in both groups of infants, B cell memory subsets were evaluated in PBMC based on expression of CD21 and CD27 on CD20+ B cells. TypP infants exhibited elevated levels of activated memory (CD21-, CD27+) B cells compared to the RP macaques (9.8-fold) at 10-12 weeks post-SIV (**Fig. 5C**). In addition to an increase in activated memory B cells in TypP infants from baseline (3.3-fold), we observed a significant decrease from baseline levels of activated memory B cells in RP infants (3-fold). The decrease in activated memory B cells in RP infants was offset by an elevation in the level of naive B cells (CD21+, CD27-) (**Fig. 5D**). Shifts in proportions of B cell subsets were restricted to naive and activated memory

compartments, as no differences were observed in proportions of resting memory (CD21+, CD27+) and tissue-like memory (CD21-, CD27-) B cells (**Fig. S3A-C**). Previous studies have identified an increase in activated memory B cells expressing CXCR3 and CD11c with chronic viral infections in mice and humans, as well as with regard to HIV-specific antibody responses (35, 36). Since a defining characteristic of the RP infants is an inability to produce SIV-specific IgG (37), we examined the association between CXCR3+ CD11c+ memory B cells and plasma anti-env IgG concentrations. The proportion of activated memory (CD27+,CD21-) B cells expressing CXCR3 and CD11c was significantly elevated in the TypP compared to the RP infant macaques (**Fig. 5E**), and expression of these two markers on activated memory B cells directly correlated with the levels of anti-SIV antibodies present at week 10-12 post-infection ($p<0.0001$) (**Fig. 5F**). These findings provide evidence that low levels of plasma anti-SIV-Env antibodies are due to insufficient memory B cell activation in RP infant macaques.

Rapidly progressing infants exhibit germinal center dysfunction in secondary lymphoid tissues. Migration of GC B cells as well as Tfh cells into follicles of lymphoid tissues is coordinated by the chemokine CXCL13 (38, 39), which is predominantly expressed by follicular dendritic cells and macrophages (38). Evaluation of plasma CXCL13 identified significantly increased concentrations in the plasma of TypP, but not RP, macaques at week 2 (1.9-fold) and weeks 4-6 (1.5-fold) compared to week 0 **(Fig. 6A**). Assessment of Tfh (CD4+ CXCR5+ PD-1hi) within the axillary lymph nodes indicated that by 3-4 weeks post-SIV, TypP infants had significantly higher levels of Tfh cells than RP infants (2.31-fold)(**Fig. 6B**). At necropsy, TypP infants experienced a significant increase in Tfh levels from the 4-6 week early chronic timepoint (3.35-fold) while RP infants experienced significant reductions (6.59-fold), resulting in dramatic differences in Tfh cell levels between the 2 groups (>50-fold difference). B cells in the lymph nodes associated with germinal centers (Ki-67+, BCL6+) were similarly elevated in TypP infants at necropsy compared to RP infants (**Fig. 6C**). The proportion of GC B cells also underwent an

209 expansion (3.09-fold) in TypP infants while contracting in RP infants (3.12-fold) during the
210 period from early chronic SIV infection until necropsy. This differential outcome resulted in 23-
211 fold higher levels of GC B cells in the TypP infants by the time of necropsy compared to RP
212 infants. To further evaluate the GC B cells (follicular, CD20+, Ki67+) their levels were assessed
213 in lymph nodes and spleen (**Fig. 6D, E**). Significantly more GC B cells were observed in splenic
214 follicles of TypP versus RP (**Fig. 6F**), however levels of GC B cells were similar within the lymph
215 nodes (**Fig. 6G**). Together these findings suggest a failure to induce functional germinal centers
216 in spleens of RP infants, while TyP infants undergo a more typical expansion of Tfh and GC B
217 cells.
218
219 **Elevated interferon-induced immune activation in lymphoid tissues and B cell follicles of**
220 **RP infants.** Type-I interferon associated immune changes have previously been described as a
221 significant factor driving pathogenesis of HIV and SIV (40-43). Assessment of plasma IFNα
222 identified sustained elevated levels within the RP macaque plasma compared to the TypP
223 macaques at both 4-6 and 10-12 weeks post-infection, with 8-fold higher concentrations of IFNα
224 in RP infants (mean 270pg/ml) compared to TyP (33 pg/ml)(**Fig. 7A**). During activation and
225 maturation, pDCs have been shown to increase expression of the costimulatory marker CD80
226 (44, 45). Therefore, pDC activation was measured as the proportion of CD80+ pDC out of total
227 CD123+/CD11c- CD14- cells using flow cytometry. We determined that while there were similar
228 levels of CD80 on circulating pDC, these levels were significantly higher in the axillary lymph
229 nodes of RP macaques, with the proportion of CD80+ pDC in RP infants doubling that of TypP
230 infants by 4-6 weeks post-SIV (**Fig 7B, C**). This finding identifies activated pDC in lymphoid
231 tissues as a potential source of elevated plasma IFNα in RP macaques.
232 To assess a direct association between elevated levels of type 1 IFN and the inability to
233 produce high levels of SIV-specific antibodies the expression of the IFN-induced protein MX1
234 was evaluated in splenic B cell follicles. While MX1 was detected in the extrafollicular area of

both TypP and RP macaques (**Fig. 8A,D**), relatively low levels of follicular MX1 production were observed in TypP infants (**Fig. 8B,C**). In contrast, RP macaques exhibited significantly increased MX1 expression in splenic germinal centers (**Fig. 8D-G**). Regions of elevated MX1 in RP infants which corresponded to sites proximal to follicles were identified as expressing a majority of SIV-infected cells by RNA-scope *in situ* hybridization (**Fig. 9A,B**). Scanning entire splenic sections determined that RP infants had significantly more SIV-positive cells/mm^2 compared to TypP infants, and that these cells are largely present in the T cell zones proximal to B cell follicles (**Fig. 9C**). These data demonstrate that increased IFN responses are observed in sites of B cell maturation in RP macaques, and that this is associated with an inability of RP infant macaques to mount SIV-specific antibody responses.

Discussion

Factors contributing to rapid progression to AIDS in infants remain poorly understood. Here, we demonstrate that 44% (11/25) of infant macaques infected with SIVmac251 between 6 and 18 months of age develop elevated SIV replication, very low or undetectable levels of SIV-specific antibodies and a more rapid disease course. Importantly, the frequency, as well as immunological, virologic, and clinical aspects of this phenotype recapitulate what has been reported in rapidly progressing HIV-infected infants (2, 4, 7, 8), and thus our findings likely reflect underlying factors driving more severe clinical outcomes. An evaluation of the immune dysfunction observed in RP infant macaques provides evidence for altered memory B cell and T follicular helper cell levels, as well as activation of lymphoid pDCs. Importantly, we have demonstrated an elevated type-I IFN-induced protein expression, similar to previous studies of rapidly progressing macaques (22, 23). The elevated type-1 IFN was observed in B cell follicles and was associated with GC dysfunction, supporting the hypothesis that aberrant IFN-driven immune activation contributes to B cell dysfunction and failure to mount humoral responses in rapidly progressing infants. An interesting finding from this study was a lack of evidence that RP

phenotype in infant macaques was associated with increased T cell activation or microbial translocation, as has been observed previously (31-33, 47). In contrast, TypP infants exhibited moderate levels of SIV plasma viremia, CD4 T cell depletion, systemic immune activation and development of hyperplastic B cell follicles more routinely associated with progression to simian AIDS (32, 48).

Identification of multiple genotypes at the initiation of infection (week 2) can be due to two possible explanations. First, there may be an increase in the number of founder viruses that infect the macaques via the oral route in the RP compared to the TypP infant macaques. Second, it is possible that increased V1V2 variants is the result of increased viral replication, and accompanying genetic mutations, due to factors intrinsic to the RP infants. Previous work from Tsai et al identified a link between rapid SIV disease progression and the number as well as relatedness of viral variants determined by sequencing of SIV*env* gene (29). This study used an R5 SHIV to infect adult female macaques intravaginally and identified a subset of macaques that failed to control viremia and developed AIDS at 30 weeks post-infection. Similar to our findings, this study found that rapidly progressing macaques had a greater number of plasma viral variants, with fewer genetic variants identified in the more typical “chronic progressors”.

While there is evidence for both expansion as well as early depletion of Tfh cells during SIV infection (53, 54), it is poorly understood whether loss of Tfh cells, and their precursors, may be attributed to direct killing from SIV or to aberrant inflammatory signaling driving apoptosis (46, 54). Selective infection of Tfh cells by HIV and SIV has been observed in both adult and infant macaques (55-58), yet rather than direct infection driving Tfh loss, infected Tfh cells are reported to serve as sanctuaries for viral persistence (55). Interestingly, adult macaques exhibiting a more rapid disease progression have trended toward lower proviral DNA levels in Tfh compared to those with more typical disease severity (54). However, while we observed similar levels of cell free virus within B cell follicle light zones (**Fig. 9**), the majority of SIV-infected cells and the brightest areas of MX1 production were observed at the periphery of

follicles (**Fig. 8**). This suggests that follicular cells do not harbor a majority of infected cells in both the RP and TypP groups. It is possible that the expression of IFN-induced proapoptotic genes (49, 59-62) during pathogenic SIV infection results in the death of Tfh cells, explaining the low level of germinal center T cells producing virus within these infant macaques.

These data allow for the elucidation of a model that summarizes our findings and outlines factors that may influence the RP phenotype outcome in the SIV infant macaques (Fig. 10). Temporally our first observation was the increase in genetic variability in SIV env V1V2 at 2 weeks post-infection (Fig. 10.1). This may be a contributing factor to, or conversely a consequence of, progression toward the RP phenotype. Viral replication drives activation of pDCs in tissue, including lymph nodes where they were observed during the late acute early chronic transition at 4-6 weeks post-infection (Fig. 10.2), The pDC activation is the likely source of elevated type 1 IFN production, which we first observe in the plasma at the same timepoint as pDC activation (Fig. 10.3). The prolonged elevated type 1 IFN could have direct effects on expansion of memory B cells and B cell function (49-51), as well as potentially influencing Tfh cell function within the lymph nodes (52) (Fig. 10.4). Germinal center dysfunction may also be influenced by failing to increase plasma concentrations of the chemokine CXCL13 (Fig. 10.5). This GC dysfunction is associated with a failure to mount an effective anti-SIV antibody responses (Fig 10.6). The findings described here therefore provide insights into the early response to the SIV infection driving outcomes toward either rapid or typical disease progression.

To summarize, these findings provide an in-depth characterization linking virological and immunological aspects of rapid SIV progression in infant macaques. Moreover, rapidly progressing macaques described here display a distinct pathology defined by failure to mount humoral immune responses and reflects key aspects of rapid progression to AIDS in infant humans. Our results also provide a detailed description of germinal center dysfunction and point to a role for aberrant IFN-signaling in germinal centers as a potential driver of this outcome.

While survival of HIV-infected infants has improved proportionally with access to antiviral therapy, early severe disease still occurs and often precedes antiretroviral therapy (63). These findings build on our understanding of infant HIV pathogenesis and can potentially be used towards the development of improved therapies and interventions.

Methods

Study Animals

All animal studies were approved by the University of Washington Animal Care and Use Committee (IACUC) under protocol #4213. 25 infant rhesus macaques were purchased and transported from the Oregon National Primate Center and were housed in the specialized infant care wing of the Washington National Primate Research Center (WaNPRC). At 5-10 weeks of age, up to 8 oral SIV challenges were administered as escalating doses ranging from 1000 TCID50 to 20000 TCID50 of SIVmac251. SIVmac251 challenges were prepared from rhesus macaque PBMC-grown supernatant, obtained from NIH AIDS Reagent Program and Dr. Nancy Miller (NIH/NIAID). Virus was diluted to 0.25 mL in RPMI1640 media and delivered dropwise across the oral mucosa via needleless syringe. Infection was confirmed by plasma viral loads (WaNPRC Virology Core). Infants that remained uninfected (plasma viral load ≤30 copies SIV RNA /mL for 2 weeks post-challenge) after 8 oral challenges were infected intravenously with 500 TCID50 of the same challenge stock (3 macaques were infected in this way) to evaluate disease pathogenesis in all infants. Infants were monitored for 9 to 12 weeks after SIV infection before being euthanized. Rhesus MHC-1 typing did not account for the frequency of rapid progression between MHC genotype and skewed susceptibility to SIV in either study group (**Table 1**).

Phenotypic Analysis of Immune Cell Subsets

Phenotypic analyses of PBMC and lymph node cell populations were performed by multiparametric flow cytometry. Freshly isolated PBMC were counted and stained as previously described (64). Briefly, activation of T cells (CD3+, CD20-, CD14-), classical monocytes (HLA-DR+, CD14+, CD16-, CD20-, CD3-) and CD16+ monocytes (HLA-DR+, CD14+, CD16+, CD20-, CD3-) was assessed using gating strategies outlined in **Figures S1 and S2.** The following antibodies were used: CD3(SP34-2)-Pacific Blue and APC, CD4(OKT4)-BV650 and APC-Cy7, CD8(SK1)-APC-H7, CD20(2H7)-BV570 and PE, CD14(M5E2)-BV785 and APC-H7, CD16(3G8)-BV605, CD11c(S-HCL-3)-APC, CD123(7G3)-PerCP-Cy5.5, CCR5(3A9)-APC, CXCR3(1C6)-PE-CF594, CD38(AT-1)-FITC, Ki-67(B65)-PE and FITC, HLA-DR(L243)-BV711 and PE, CD80(L307.4)-PE-Cy7, CD83(HB15e)-PE-CF594, CD86(2331)-BV711 (BD Life Sciences). Stained cells were washed and fixed in 1% paraformaldehyde before analysis on a LSR-II flow cytometer (BD Biosciences). Compensation and analysis were performed using FlowJo version 10 (v. 10.5.3, FlowJo LLC)

Analysis of plasma protein and IgG/IgA concentrations

Plasma samples were collected after centrifugation of whole blood collected in EDTA tubes. Plasma IFNα concentrations were measured with the Human IFN-α ELISA^{PRO}kit (Mabtech), following the manufacturer's instructions. Plasma CXCL13 was measured using a Human BLC ELISA kit (Ray Biotech). Plasma sCD14 was measured using the Human CD14 Quantikine ELISA kit (R&D Systems). Plasma LPS binding protein (LBP) was measured using an LBP quantification immunoassay (Biometec). Measurement of plasma anti-SIVgp140 IgG and IgA concentrations was performed using a custom ELISA containing wells coated with rGP130 (NIH-ARP #12797). Samples were serially diluted and absorbance values were fit to standard curves generated using either purified rhesus IgG or IgA.

SIV env sequence analysis

Viral RNA was isolated from rhesus macaque plasma from 2 weeks post-SIV infection using an Ultrasense Viral RNA kit (QIAGEN) and cDNA was reverse transcribed using the Applied Biosystems High Capacity cDNA synthesis kit (Thermo-Fisher). Libraries were prepared using a 2 step PCR protocol for amplifying the 584bp product with adaptors. First round primers: F: TAGAGGATGTATGGCAACTC and R: CTTGTGCATGAAGAGACCA. Second round primers: F: TCGTCGGCAGCGTCAGATGTGTATAAGAGACAGTATGGCAACTCTTTGAGACC and R: GTCTCGTGGGCTCGGAGATGTGTATAAGAGACAGGAAGAGACCACCACCTTAG. PCR products were FLASH-gel purified and a 5-cycle indexing PCR was used for addition of P5 and P7 Illumina indices. Libraries were loaded onto an Illumina 600 cycle V3 cartridge according to the manufacturer's instructions and run on an Illumina MiSeq as described previously (65). Amplicons were reconstructed from forward and reverse FASTQ reads via FLASH with maximum and minimum parameters set so that >95% of reads were aligned. Adaptor sequences were removed using cutadapt with error rate of 0.3 and minimum length of 100bp. Sequence quality filters were applied using FASTQ_quality_filter with a minimum quality score of 20, and the minimum percent of bases that must have the set minimum quality score to 100%. Duplicates were removed using dedupe2.sh, allowing for maximum mismatches of 5 and maximum edits set to 2. In individual plasma samples from infants infected by oral challenge, this approach provided an average of 258 thousand sequences after filtering paired reads based on quality score. After collapsing identical sequences, unique variant clusters were identified as a set of sequences with no more than 5bp mismatches among them. Additionally, these unique variants were present at levels of at least 10 copies to be considered for further analysis. Fastq files were converted to fasta and aligned with Clustal Ω and unique genotypes were enumerated. Alignments were uploaded to the DIVEIN analysis server where phylogenies were constructed by maximum likelihood using the generalized time reversal substitution model (66). Pairwise distance was calculated using a consensus sequence derived from the 331 sequenced V1V2 variants represented within our SIVmac251 challenge stock.

Tissue imaging

Immunofluorescence microscopy was carried out as previously described (67), with the following exceptions: B cells were targeted using α-CD20 (clone EP459Y, Abcam, 1:300); proliferating cells were targeted using anti-Ki-67 (clone MM1, Leica Biosystems, 1:100); cells responding to IFN signaling were targeted by anti-Mx1 (clone M143, EMD Millipore, 1:500). CD20 was detected using goat anti-rabbit Alexa Fluor 594 (Life Technologies, 1:500) while Ki-67 and Mx1 were detected using goat anti-mouse Alexa Fluor 488 (Life Technologies, 1:500). Spleen and lymph node and sections were scanned under 100x magnification using a Nikon Eclipse Ti inverted fluorescent microscope (Nikon, Melville, NY) to capture and stitch multiple fields. Analysis was carried out on ten randomly selected B cell follicles per tissue. Quantification of Ki-67 was carried out in Imaris software by manually selecting follicles followed by counting Ki-67 using the spots tool. Mx1 was quantified in Fiji by selecting B cell follicles and thresholding a mask using the “Moments” parameters followed by counting the number of Mx1 positive and Mx1 negative pixels to calculate percent of pixels positive for Mx1.

In situ hybridization analysis of SIV RNA in the spleen was carried out as previously described (67). Assays were carried out using RNAscope technology (Advanced Cell Diagnostics). Spleen sections (5μm) on glass slides were baked at 60˚C for 1 hour before deparaffinization in xylene (2 × 5 minutes) followed by 100% ethanol (2 × 3 minutes). Slides were then pretreated with hydrogen peroxide reagent to quench endogenous peroxidases. Antigen retrieval was performed by boiling slides for 20 minutes in antigen retrieval buffer followed by washing in deionized water and ethanol and baking for 30 minutes at 60˚C. SIVmac239 probes (Advanced Cell Diagnostics) targeting SIV gag, pol, tat, rev, env, vpx, vpr, nef and rev genes were then hybridized to tissue for 2 hours at 40˚C. Following the recommended six amplification steps, DAB-A and B reagents were mixed and incubated with tissue until visual detection of brown color was achieved. Tissues were counterstained with CAT

Hematoxylin for 30 seconds and briefly rinsed with tap H_2O. Coverslips were mounted using Permount mounting media and allowed to cure overnight before imaging. Scanned images of whole mounted tissue cross sections were acquired as described above. SIV+ cells were quantified in FIJI software by color thresholding followed by the particle analysis tool with size parameters adjusted to detect only cells.

Statistical Analysis

All statistical analyses were performed using either Prism v.8 (Graph Pad) or R version 3.5.1. Data distributions were assessed using D'Agostino and Pearson normality tests. Comparisons of proportions of immune cell populations and cytokines across and between TypP and RP infants were made using 2-tailed Mann–Whitney U tests, Wilcoxen matched-pairs signed-ranks tests, or t-tests when appropriate.

Acknowledgements This work was supported in part by the following National Institutes of Health awards: R01-DE023047 and R01 AI133706. This work was also supported by the University of Washington Pathobiology Training Grant T32-A1750915. The Washington National Primate Center is supported by grant P51 OD010425 from the NIH Office of Research Infrastructure Programs. The authors would also like to acknowledge the veterinary and support staff at the Washington National Primate Research Center and LaRene Kuller and Richard Grant for support with RNA processing for Nanostring analysis, Brian Johnson at the University of Washington Histology and Imaging Core for expertise and technical assistance and Roger Wiseman and Eileen Maher at the University of Wisconsin Madison and the Wisconsin National Primate Research Center for assistance with MHC typing.

Author Contributions:

Conceptualization: MPW, DLS, AC, DHF

Data Curation: MPW, CIJ, KAF, BGO

Formal Analysis: MPW, CIJ, KAF, JTF

Funding Acquisition: DLS, DHF

Investigation: MPW, CIJ, KAF, JTF, JH, MM, BSF, PM, PJW

Methodology: BGO, NS, MM, MPW, CIJ, PJW

Project Administration: MPW, AC, DLS, NS

Resources: NS, DHF,

Software: MPW, KAF

Supervision: MPW, DLS, AC

Validation: MPW, MM, BGO

Visualization: MPW, DLS

Writing – Original Draft Preparation: MPW, DLS, CIJ

Writing – Review and Editing: MPW, MM, AC, DLS, DHF

References

1. UNAIDS. AIDSinfo 2019 [cited 2019. Available from: aidsinfo.unaids.org.

2. Newell ML, Coovadia H, Cortina-Borja M, Rollins N, Gaillard P, Dabis F, et al. Mortality of infected and uninfected infants born to HIV-infected mothers in Africa: a pooled analysis. Lancet. 2004;364(9441):1236-43, 10.1016/S0140-6736(04)17140-7, https://www.ncbi.nlm.nih.gov/pubmed/15464184.

3. Espanol T, Garcia-Armui R, Bofill A, Sune J, Bertran JM. Hypogammaglobulinaemia and negative anti-HIV antibodies in AIDS. Arch Dis Child. 1987;62(8):853-4, 10.1136/adc.62.8.853, https://www.ncbi.nlm.nih.gov/pubmed/3662596.

4. Pahwa R, Good RA, Pahwa S. Prematurity, hypogammaglobulinemia, and neuropathology with human immunodeficiency virus (HIV) infection. Proc Natl Acad Sci U S A. 1987;84(11):3826-30, 10.1073/pnas.84.11.3826, https://www.ncbi.nlm.nih.gov/pubmed/3473485.

5. Gaetano C, Scano G, Carbonari M, Giannini G, Mezzaroma I, Aiuti F, et al. Delayed and defective anti-HIV IgM response in infants. Lancet. 1987;1(8533):631, 10.1016/s0140-6736(87)90272-8, https://www.ncbi.nlm.nih.gov/pubmed/2881166.

6. Goulder PJ, Jeena P, Tudor-Williams G, Burchett S. Paediatric HIV infection: correlates of protective immunity and global perspectives in prevention and management. Br Med Bull. 2001;58:89-108, 10.1093/bmb/58.1.89, https://www.ncbi.nlm.nih.gov/pubmed/11714626.

7. Tovo PA, de Martino M, Gabiano C, Cappello N, D'Elia R, Loy A, et al. Prognostic factors and survival in children with perinatal HIV-1 infection. The Italian Register for HIV Infections in Children. Lancet. 1992;339(8804):1249-53, 10.1016/0140-6736(92)91592-v, https://www.ncbi.nlm.nih.gov/pubmed/1349667.

8. Pahwa S, Kaplan M, Fikrig S, Pahwa R, Sarngadharan MG, Popovic M, et al. Spectrum of human T-cell lymphotropic virus type III infection in children. Recognition of symptomatic, asymptomatic, and seronegative patients. JAMA. 1986;255(17):2299-305, https://www.ncbi.nlm.nih.gov/pubmed/3007791.

9. Stacey AR, Norris PJ, Qin L, Haygreen EA, Taylor E, Heitman J, et al. Induction of a striking systemic cytokine cascade prior to peak viremia in acute human immunodeficiency virus type 1 infection, in contrast to more modest and delayed responses in acute hepatitis B

and C virus infections. J Virol. 2009;83(8):3719-33, 10.1128/JVI.01844-08, https://www.ncbi.nlm.nih.gov/pubmed/19176632.

10. Moir S, Chun TW, Fauci AS. Pathogenic mechanisms of HIV disease. Annu Rev Pathol. 2011;6:223-48, 10.1146/annurev-pathol-011110-130254, https://www.ncbi.nlm.nih.gov/pubmed/21034222.

11. Cohen MS, Shaw GM, McMichael AJ, Haynes BF. Acute HIV-1 Infection. N Engl J Med. 2011;364(20):1943-54, 10.1056/NEJMra1011874, https://www.ncbi.nlm.nih.gov/pubmed/21591946.

12. Tomaras GD, Haynes BF. HIV-1-specific antibody responses during acute and chronic HIV-1 infection. Curr Opin HIV AIDS. 2009;4(5):373-9, 10.1097/COH.0b013e32832f00c0, https://www.ncbi.nlm.nih.gov/pubmed/20048700.

13. Goulder PJ, Lewin SR, Leitman EM. Paediatric HIV infection: the potential for cure. Nat Rev Immunol. 2016;16(4):259-71, 10.1038/nri.2016.19, https://www.ncbi.nlm.nih.gov/pubmed/26972723.

14. Prendergast AJ, Chasekwa B, Rukobo S, Govha M, Mutasa K, Ntozini R, et al. Intestinal Damage and Inflammatory Biomarkers in Human Immunodeficiency Virus (HIV)-Exposed and HIV-Infected Zimbabwean Infants. J Infect Dis. 2017;216(6):651-61, 10.1093/infdis/jix367, https://www.ncbi.nlm.nih.gov/pubmed/28934432.

15. Pananghat AN, Aggarwal H, Prakash SS, Makhdoomi MA, Singh R, Lodha R, et al. IL-8 Alterations in HIV-1 Infected Children With Disease Progression. Medicine (Baltimore). 2016;95(21):e3734, 10.1097/MD.0000000000003734, https://www.ncbi.nlm.nih.gov/pubmed/27227934.

508 16. Baba TW, Jeong YS, Pennick D, Bronson R, Greene MF, Ruprecht RM. Pathogenicity of
509 live, attenuated SIV after mucosal infection of neonatal macaques. Science.
510 1995;267(5205):1820-5, 10.1126/science.7892606,
511 https://www.ncbi.nlm.nih.gov/pubmed/7892606.
512 17. Marthas ML, van Rompay KK, Otsyula M, Miller CJ, Canfield DR, Pedersen NC, et al. Viral
513 factors determine progression to AIDS in simian immunodeficiency virus-infected newborn
514 rhesus macaques. J Virol. 1995;69(7):4198-205, 10.1128/JVI.69.7.4198-4205.1995,
515 https://www.ncbi.nlm.nih.gov/pubmed/7769679.
516 18. Abel K, Pahar B, Van Rompay KK, Fritts L, Sin C, Schmidt K, et al. Rapid virus
517 dissemination in infant macaques after oral simian immunodeficiency virus exposure in the
518 presence of local innate immune responses. J Virol. 2006;80(13):6357-67, 10.1128/JVI.02240-
519 05, https://www.ncbi.nlm.nih.gov/pubmed/16775324.
520 19. Chakraborty R. HIV-1 infection in children: a clinical and immunologic overview. Curr HIV
521 Res. 2005;3(1):31-41, 10.2174/1570162052773022,
522 https://www.ncbi.nlm.nih.gov/pubmed/15638721.
523 20. Wang X, Xu H, Pahar B, Alvarez X, Green LC, Dufour J, et al. Simian immunodeficiency
524 virus selectively infects proliferating CD4+ T cells in neonatal rhesus macaques. Blood.
525 2010;116(20):4168-74, 10.1182/blood-2010-03-273482,
526 https://www.ncbi.nlm.nih.gov/pubmed/20716768.
527 21. Milush JM, Kosub D, Marthas M, Schmidt K, Scott F, Wozniakowski A, et al. Rapid
528 dissemination of SIV following oral inoculation. AIDS. 2004;18(18):2371-80,
529 https://www.ncbi.nlm.nih.gov/pubmed/15622313.

530 22. Durudas A, Milush JM, Chen HL, Engram JC, Silvestri G, Sodora DL. Elevated levels of
531 innate immune modulators in lymph nodes and blood are associated with more-rapid disease
532 progression in simian immunodeficiency virus-infected monkeys. J Virol. 2009;83(23):12229-40,
533 10.1128/JVI.01311-09, https://www.ncbi.nlm.nih.gov/pubmed/19759147.
534 23. Easlick J, Szubin R, Lantz S, Baumgarth N, Abel K. The early interferon alpha subtype
535 response in infant macaques infected orally with SIV. J Acquir Immune Defic Syndr.
536 2010;55(1):14-28, 10.1097/QAI.0b013e3181e696ca,
537 https://www.ncbi.nlm.nih.gov/pubmed/20616742.
538 24. Letvin NL, King NW. Immunologic and pathologic manifestations of the infection of
539 rhesus monkeys with simian immunodeficiency virus of macaques. J Acquir Immune Defic Syndr
540 (1988). 1990;3(11):1023-40, https://www.ncbi.nlm.nih.gov/pubmed/2213505.
541 25. Otsyula MG, Miller CJ, Marthas ML, Van Rompay KK, Collins JR, Pedersen NC, et al. Virus-
542 induced immunosuppression is linked to rapidly fatal disease in infant rhesus macaques
543 infected with simian immunodeficiency virus. Pediatr Res. 1996;39(4 Pt 1):630-5,
544 10.1203/00006450-199604000-00012, https://www.ncbi.nlm.nih.gov/pubmed/8848337.
545 26. Dykhuizen M, Mitchen JL, Montefiori DC, Thomson J, Acker L, Lardy H, et al.
546 Determinants of disease in the simian immunodeficiency virus-infected rhesus macaque:
547 characterizing animals with low antibody responses and rapid progression. J Gen Virol. 1998;79
548 (Pt 10):2461-7, 10.1099/0022-1317-79-10-2461,
549 https://www.ncbi.nlm.nih.gov/pubmed/9780052.
550 27. Titanji K, Velu V, Chennareddi L, Vijay-Kumar M, Gewirtz AT, Freeman GJ, et al. Acute
551 depletion of activated memory B cells involves the PD-1 pathway in rapidly progressing SIV-

552 infected macaques. J Clin Invest. 2010;120(11):3878-90, 10.1172/JCI43271,
553 https://www.ncbi.nlm.nih.gov/pubmed/20972331.
554 28. Brown CR, Czapiga M, Kabat J, Dang Q, Ourmanov I, Nishimura Y, et al. Unique
555 pathology in simian immunodeficiency virus-infected rapid progressor macaques is consistent
556 with a pathogenesis distinct from that of classical AIDS. J Virol. 2007;81(11):5594-606,
557 10.1128/JVI.00202-07, https://www.ncbi.nlm.nih.gov/pubmed/17376901.
558 29. Tsai L, Tasovski I, Leda AR, Chin MP, Cheng-Mayer C. The number and genetic
559 relatedness of transmitted/founder virus impact clinical outcome in vaginal R5 SHIVSF162P3N
560 infection. Retrovirology. 2014;11:22, 10.1186/1742-4690-11-22,
561 https://www.ncbi.nlm.nih.gov/pubmed/24612462.
562 30. Liu Z, Cumberland WG, Hultin LE, Prince HE, Detels R, Giorgi JV. Elevated CD38 antigen
563 expression on CD8+ T cells is a stronger marker for the risk of chronic HIV disease progression
564 to AIDS and death in the Multicenter AIDS Cohort Study than CD4+ cell count, soluble immune
565 activation markers, or combinations of HLA-DR and CD38 expression. J Acquir Immune Defic
566 Syndr Hum Retrovirol. 1997;16(2):83-92, 10.1097/00042560-199710010-00003,
567 https://www.ncbi.nlm.nih.gov/pubmed/9358102.
568 31. Brenchley JM, Price DA, Schacker TW, Asher TE, Silvestri G, Rao S, et al. Microbial
569 translocation is a cause of systemic immune activation in chronic HIV infection. Nat Med.
570 2006;12(12):1365-71, 10.1038/nm1511, https://www.ncbi.nlm.nih.gov/pubmed/17115046.
571 32. Bosinger SE, Sodora DL, Silvestri G. Generalized immune activation and innate immune
572 responses in simian immunodeficiency virus infection. Curr Opin HIV AIDS. 2011;6(5):411-8,
573 10.1097/COH.0b013e3283499cf6, https://www.ncbi.nlm.nih.gov/pubmed/21743324.

574 33. Burgener A, McGowan I, Klatt NR. HIV and mucosal barrier interactions: consequences
575 for transmission and pathogenesis. Curr Opin Immunol. 2015;36:22-30,
576 10.1016/j.coi.2015.06.004, https://www.ncbi.nlm.nih.gov/pubmed/26151777.
577 34. Malaspina A, Moir S, Kottilil S, Hallahan CW, Ehler LA, Liu S, et al. Deleterious effect of
578 HIV-1 plasma viremia on B cell costimulatory function. J Immunol. 2003;170(12):5965-72,
579 10.4049/jimmunol.170.12.5965, https://www.ncbi.nlm.nih.gov/pubmed/12794123.
580 35. Barnett BE, Staupe RP, Odorizzi PM, Palko O, Tomov VT, Mahan AE, et al. Cutting Edge: B
581 Cell-Intrinsic T-bet Expression Is Required To Control Chronic Viral Infection. J Immunol.
582 2016;197(4):1017-22, 10.4049/jimmunol.1500368,
583 https://www.ncbi.nlm.nih.gov/pubmed/27430722.
584 36. Knox JJ, Buggert M, Kardava L, Seaton KE, Eller MA, Canaday DH, et al. T-bet+ B cells are
585 induced by human viral infections and dominate the HIV gp140 response. JCI Insight. 2017;2(8),
586 10.1172/jci.insight.92943, https://www.ncbi.nlm.nih.gov/pubmed/28422752.
587 37. Muehlinghaus G, Cigliano L, Huehn S, Peddinghaus A, Leyendeckers H, Hauser AE, et al.
588 Regulation of CXCR3 and CXCR4 expression during terminal differentiation of memory B cells
589 into plasma cells. Blood. 2005;105(10):3965-71, 10.1182/blood-2004-08-2992,
590 https://www.ncbi.nlm.nih.gov/pubmed/15687242.
591 38. Wang X, Cho B, Suzuki K, Xu Y, Green JA, An J, et al. Follicular dendritic cells help
592 establish follicle identity and promote B cell retention in germinal centers. J Exp Med.
593 2011;208(12):2497-510, 10.1084/jem.20111449,
594 https://www.ncbi.nlm.nih.gov/pubmed/22042977.

595 39. Havenar-Daughton C, Lindqvist M, Heit A, Wu JE, Reiss SM, Kendric K, et al. CXCL13 is a
596 plasma biomarker of germinal center activity. Proc Natl Acad Sci U S A. 2016;113(10):2702-7,
597 10.1073/pnas.1520112113, https://www.ncbi.nlm.nih.gov/pubmed/26908875.
598 40. Bosinger SE, Li Q, Gordon SN, Klatt NR, Duan L, Xu L, et al. Global genomic analysis
599 reveals rapid control of a robust innate response in SIV-infected sooty mangabeys. J Clin Invest.
600 2009;119(12):3556-72, 10.1172/JCI40115, https://www.ncbi.nlm.nih.gov/pubmed/19959874.
601 41. Jacquelin B, Mayau V, Targat B, Liovat AS, Kunkel D, Petitjean G, et al. Nonpathogenic
602 SIV infection of African green monkeys induces a strong but rapidly controlled type I IFN
603 response. J Clin Invest. 2009;119(12):3544-55, 10.1172/JCI40093,
604 https://www.ncbi.nlm.nih.gov/pubmed/19959873.
605 42. Harris LD, Tabb B, Sodora DL, Paiardini M, Klatt NR, Douek DC, et al. Downregulation of
606 robust acute type I interferon responses distinguishes nonpathogenic simian immunodeficiency
607 virus (SIV) infection of natural hosts from pathogenic SIV infection of rhesus macaques. J Virol.
608 2010;84(15):7886-91, 10.1128/JVI.02612-09,
609 https://www.ncbi.nlm.nih.gov/pubmed/20484518.
610 43. Hardy GA, Sieg S, Rodriguez B, Anthony D, Asaad R, Jiang W, et al. Interferon-alpha is the
611 primary plasma type-I IFN in HIV-1 infection and correlates with immune activation and disease
612 markers. PLoS One. 2013;8(2):e56527, 10.1371/journal.pone.0056527,
613 https://www.ncbi.nlm.nih.gov/pubmed/23437155.
614 44. Ito T, Yang M, Wang YH, Lande R, Gregorio J, Perng OA, et al. Plasmacytoid dendritic
615 cells prime IL-10-producing T regulatory cells by inducible costimulator ligand. J Exp Med.

2007;204(1):105-15, 10.1084/jem.20061660,
https://www.ncbi.nlm.nih.gov/pubmed/17200410.

45. Banchereau J, Briere F, Caux C, Davoust J, Lebecque S, Liu YJ, et al. Immunobiology of dendritic cells. Annu Rev Immunol. 2000;18:767-811, 10.1146/annurev.immunol.18.1.767, https://www.ncbi.nlm.nih.gov/pubmed/10837075.

46. Xu H, Wang X, Malam N, Lackner AA, Veazey RS. Persistent Simian Immunodeficiency Virus Infection Causes Ultimate Depletion of Follicular Th Cells in AIDS. J Immunol. 2015;195(9):4351-7, 10.4049/jimmunol.1501273, https://www.ncbi.nlm.nih.gov/pubmed/26408660.

47. Hirsch VM, Martin JE, Dapolito G, Elkins WR, London WT, Goldstein S, et al. Spontaneous substitutions in the vicinity of the V3 analog affect cell tropism and pathogenicity of simian immunodeficiency virus. J Virol. 1994;68(4):2649-61, 10.1128/JVI.68.4.2649-2661.1994, https://www.ncbi.nlm.nih.gov/pubmed/8139042.

48. Brocca-Cofano E, Kuhrt D, Siewe B, Xu C, Haret-Richter GS, Craigo J, et al. Pathogenic Correlates of Simian Immunodeficiency Virus-Associated B Cell Dysfunction. J Virol. 2017;91(23), 10.1128/JVI.01051-17, https://www.ncbi.nlm.nih.gov/pubmed/28931679.

49. Moir S, Malaspina A, Pickeral OK, Donoghue ET, Vasquez J, Miller NJ, et al. Decreased survival of B cells of HIV-viremic patients mediated by altered expression of receptors of the TNF superfamily. J Exp Med. 2004;200(7):587-99, https://www.ncbi.nlm.nih.gov/pubmed/15508184.

636 50. Peters M, Ambrus JL, Zheleznyak A, Walling D, Hoofnagle JH. Effect of interferon-alpha
637 on immunoglobulin synthesis by human B cells. J Immunol. 1986;137(10):3153-7,
638 https://www.ncbi.nlm.nih.gov/pubmed/3021846.
639 51. Oka H, Hirohata S, Inoue T, Ito K. Effects of interferon-alpha on human B cell
640 responsiveness: biphasic effects in cultures stimulated with Staphylococcus aureus. Cell
641 Immunol. 1992;139(2):478-92, 10.1016/0008-8749(92)90087-6,
642 https://www.ncbi.nlm.nih.gov/pubmed/1346369.
643 52. Cubas RA, Mudd JC, Savoye AL, Perreau M, van Grevenynghe J, Metcalf T, et al.
644 Inadequate T follicular cell help impairs B cell immunity during HIV infection. Nat Med.
645 2013;19(4):494-9, 10.1038/nm.3109, https://www.ncbi.nlm.nih.gov/pubmed/23475201.
646 53. Petrovas C, Yamamoto T, Gerner MY, Boswell KL, Wloka K, Smith EC, et al. CD4 T
647 follicular helper cell dynamics during SIV infection. J Clin Invest. 2012;122(9):3281-94,
648 10.1172/JCI63039, https://www.ncbi.nlm.nih.gov/pubmed/22922258.
649 54. Moukambi F, Rabezanahary H, Rodrigues V, Racine G, Robitaille L, Krust B, et al. Early
650 Loss of Splenic Tfh Cells in SIV-Infected Rhesus Macaques. PLoS Pathog. 2015;11(12):e1005287,
651 10.1371/journal.ppat.1005287, https://www.ncbi.nlm.nih.gov/pubmed/26640894.
652 55. Rabezanahary H, Moukambi F, Palesch D, Clain J, Racine G, Andreani G, et al. Despite
653 early antiretroviral therapy effector memory and follicular helper CD4 T cells are major
654 reservoirs in visceral lymphoid tissues of SIV-infected macaques. Mucosal Immunol.
655 2020;13(1):149-60, 10.1038/s41385-019-0221-x,
656 https://www.ncbi.nlm.nih.gov/pubmed/31723251.

657 56. Fukazawa Y, Lum R, Okoye AA, Park H, Matsuda K, Bae JY, et al. B cell follicle sanctuary
658 permits persistent productive simian immunodeficiency virus infection in elite controllers. Nat
659 Med. 2015;21(2):132-9, 10.1038/nm.3781, https://www.ncbi.nlm.nih.gov/pubmed/25599132.
660 57. Mavigner M, Habib J, Deleage C, Rosen E, Mattingly C, Bricker K, et al. Simian
661 Immunodeficiency Virus Persistence in Cellular and Anatomic Reservoirs in Antiretroviral
662 Therapy-Suppressed Infant Rhesus Macaques. J Virol. 2018;92(18), 10.1128/JVI.00562-18,
663 https://www.ncbi.nlm.nih.gov/pubmed/29997216.
664 58. Obregon-Perko V, Bricker K, Mensah G, Uddin F, Kumar M, Fray E, et al. SHIV.C.CH505
665 Persistence in ART-Suppressed Infant Macaques is Characterized by Elevated SHIV RNA in the
666 Gut and High Abundance of Intact SHIV DNA in Naive CD4+ T cells. J Virol. 2020,
667 10.1128/JVI.01669-20, https://www.ncbi.nlm.nih.gov/pubmed/33087463.
668 59. van Grevenynghe J, Cubas RA, Noto A, DaFonseca S, He Z, Peretz Y, et al. Loss of
669 memory B cells during chronic HIV infection is driven by Foxo3a- and TRAIL-mediated apoptosis.
670 J Clin Invest. 2011;121(10):3877-88, 10.1172/JCI59211,
671 https://www.ncbi.nlm.nih.gov/pubmed/21926463.
672 60. Katsikis PD, Wunderlich ES, Smith CA, Herzenberg LA, Herzenberg LA. Fas antigen
673 stimulation induces marked apoptosis of T lymphocytes in human immunodeficiency virus-
674 infected individuals. J Exp Med. 1995;181(6):2029-36, 10.1084/jem.181.6.2029,
675 https://www.ncbi.nlm.nih.gov/pubmed/7539037.
676 61. Laforge M, Campillo-Gimenez L, Monceaux V, Cumont MC, Hurtrel B, Corbeil J, et al.
677 HIV/SIV infection primes monocytes and dendritic cells for apoptosis. PLoS Pathog.

678 2011;7(6):e1002087, 10.1371/journal.ppat.1002087,

679 https://www.ncbi.nlm.nih.gov/pubmed/21731488.

680 62. Fraietta JA, Mueller YM, Yang G, Boesteanu AC, Gracias DT, Do DH, et al. Type I

681 interferon upregulates Bak and contributes to T cell loss during human immunodeficiency virus

682 (HIV) infection. PLoS Pathog. 2013;9(10):e1003658, 10.1371/journal.ppat.1003658,

683 https://www.ncbi.nlm.nih.gov/pubmed/24130482.

684 63. Innes S, Lazarus E, Otwombe K, Liberty A, Germanus R, Van Rensburg AJ, et al. Early

685 severe HIV disease precedes early antiretroviral therapy in infants: Are we too late? J Int AIDS

686 Soc. 2014;17:18914, 10.7448/IAS.17.1.18914,

687 https://www.ncbi.nlm.nih.gov/pubmed/24925044.

688 64. Wood MP, Wood LF, Templeton M, Fisher B, Lippy A, Jones CI, et al. Transient Immune

689 Activation in BCG-Vaccinated Infant Rhesus Macaques Is Not Sufficient to Influence Oral Simian

690 Immunodeficiency Virus Infection. J Infect Dis. 2020;222(1):44-53, 10.1093/infdis/jiz382,

691 https://www.ncbi.nlm.nih.gov/pubmed/31605528.

692 65. Vigdorovich V, Oliver BG, Carbonetti S, Dambrauskas N, Lange MD, Yacoob C, et al.

693 Repertoire comparison of the B-cell receptor-encoding loci in humans and rhesus macaques by

694 next-generation sequencing. Clin Transl Immunology. 2016;5(7):e93, 10.1038/cti.2016.42,

695 https://www.ncbi.nlm.nih.gov/pubmed/27525066.

696 66. Deng W, Maust BS, Nickle DC, Learn GH, Liu Y, Heath L, et al. DIVEIN: a web server to

697 analyze phylogenies, sequence divergence, diversity, and informative sites. Biotechniques.

698 2010;48(5):405-8, 10.2144/000113370, https://www.ncbi.nlm.nih.gov/pubmed/20569214.

699 67. Fisher BS, Green RR, Brown RR, Wood MP, Hensley-McBain T, Fisher C, et al. Liver
700 macrophage-associated inflammation correlates with SIV burden and is substantially reduced
701 following cART. PLoS Pathog. 2018;14(2):e1006871, 10.1371/journal.ppat.1006871,
702 https://www.ncbi.nlm.nih.gov/pubmed/29466439.

703

704 **Figure 1: SIV-infected infant macaques exhibit disparate anti-SIV IgG responses.** Infants
705 were infected with SIVmac251 either orally (n=22) or intravenously (n=3) with SIVmac251 and
706 viral load and production of anti gp120 antibodies was monitored until necropsy at 10–22 weeks
707 post infection. 15 of 25 infants that did not produce anti-gp140 specific plasma IgG or IgA during
708 chronic SIV infection (10-12 weeks post-SIV infection) and were characterized as Rapid
709 Progressors (**RP**)(**A,B**). RP infants failed to reduce plasma viral load after acute infection and
710 maintained higher viral loads during chronic infection (**D,E**). Typical progressors (**TypP**) are
711 represented as **closed circles** and RP infants are represented as **open squares**. Statistical
712 tests used to compare infant groups were carried out as described in the methods ** = p<0.01,
713 *** = p<0.001, ****= p<0.0001. Error bars are shown as either mean with standard deviation or
714 median with interquartile range based on data distribution.

715

716 **Figure 2: Number of unique plasma viral variants detected at week 2 post infection**
717 **negatively correlates with anti-SIV antibodies at wk10.** SIV viral variants were assessed at 2
718 weeks post-infection from plasma viral RNA on an Illumina MiSeq platform. Representative
719 phylogenies are shown for TypP (**A**) and RP (**B**) infants. The total number of unique plasma
720 viral variants was quantified and compared between TypP (**closed circles**) and RP (**open**
721 **squares**) infants (**C**). Number of viral variants were compared against plasma anti-SIVenv IgG
722 concentration (**D**). Phylogenies were constructed using maximum likelihood with a GTR
723 substitution model. Black lines in trees represent challenge stock consensus sequence.

Statistical tests used to compare infant groups were carried out as described in the methods * = p<0.05. Error bars are shown as either mean with standard deviation or median with interquartile range based on data distribution.

Figure 3: Total CD4 T cell levels are sustained during chronic infection in RP infants. CD4 T cell depletion was monitored over time using a CD4/CD8 ratio in PBMC from TypP (**closed circles**) and RP (**open squares**) infants (**A,B**). The total number of peripheral CD4 T cells was monitored following SIV infection (**C**). Statistical tests used to compare infant groups were carried out as described in the methods * = p<0.05, ** = p<0.01, *** = p<0.001. Error bars are shown as either mean with standard deviation or median with interquartile range based on data distribution.

Figure 4: Activation of CD4 and CD8 T cells is increased in typically progressing infants. Levels of HLA-DR+ CD4 (**A**) and CD8 (**B**) T cells in peripheral blood were evaluated in TypP (closed circles) and RP (open squares) infants. Both paired and unpaired and parametric and nonparametric tests were used to compare groups depending on the distribution of the data. ** = p<0.01, *** = p<0.001, ****= p<0.0001. Error bars are shown as either mean with standard deviation or median with interquartile range based on data distribution.

Figure 5: Rapidly progressing infants fail to increase activated memory B cells during chronic infection. Proportions of CD20+ B cells (**A**) as well as CD80+ activated B cells (**B**) are shown from PBMC of TypP (closed circles) and RP (open squares) infants. Proportions of activated memory (**C**) and naïve (**D**) B cell populations from total CD20+ B cells are also compared between TypP and RP infants. Within activated memory B cells we compared atypical CD11c, CXCR3 double positive cells in both TypP and RP infants (**E**) and correlations with anti-SIV antibody levels are shown at week 10-12 (**F**). Statistical tests used to compare infant groups were carried out as described in the methods ** = p<0.01, *** = p<0.001, ****=

p<0.0001. Error bars are shown as either mean with standard deviation or median with interquartile range based on data distribution.

Figure 6: Rapidly progressing infants exhibit germinal center dysfunction in secondary lymphoid tissues. Plasma CXCL13 concentrations were measured at timepoints prior to and following SIV infection in TypP (**closed circles**) and RP (**open squares**) infants (**A)** Levels of T follicular helper cells(CXCR5+, PD-1+)(**B**) and germinal center B cells (Ki-67+, BcL6+)(**C**) were measured in axillary lymph node biopsies from early chronic (4-6 weeks post-infection) and necropsy. Paraffin embedded spleens from RP and TypP infants were sectioned and immuno-stained for B cells (CD20, red) proliferation (Ki-67, green) to identify splenic B cell follicles and germinal centers. Representative images are shown for TypP infants (**D**) and RP infants (**E**). Whole sections were scanned and stitched, and Ki-67 positive foci were quantified in B cell follicles of spleen (**F**) and axillary lymph node (**G**). Statistical tests used to compare infant groups were carried out as described in the methods ** = p<0.01. Error bars are shown as either mean with standard deviation or median with interquartile range based on data distribution.

Figure 7: Elevated Interferon-α and pDC activation in RP infants. Plasma IFNα concentrations were measured by ELISA at multiple time points in TypP and RP infants (**A**). Proportions of activated CD80+ plasmacytoid dendritic (CD163+) in PBMC from TypP (**closed circles**) and RP (**open squares**) infants were evaluated in blood (**B**) and lymph nodes (**C**) by flow cytometry. Statistical tests used to compare infant groups were carried out as described in the methods * = p<0.05, *** = p<0.001, ****= p<0.0001. Error bars are shown as either mean with standard deviation or median with interquartile range based on data distribution.

Figure 8: Increased type 1 IFN associated protein expression is observed in B cell follicles of RP infants. Levels of MX1 protein were measured in areas within B cell follicles of spleen. Paraffin embedded spleens from RP and TypP infants were sectioned and immuno-stained for B cells (CD20, red) and MX1 (green) to identify splenic B cell follicles and IFN-induced protein expression. Representative images are shown for TypP infants (**A-C**) and RP infants (**D-F**). Whole sections were scanned and stitched and MX1 was quantified within 10 randomly selected splenic B cell follicles (**G**) for TypP (**closed circles**) and RP (**open squares**) infants. Statistical tests used to compare infant groups were carried out as described in the methods * = $p<0.05$

Figure 9: Rapidly progressing infants have more SIV infected cells localized outside of splenic germinal centers. RNAscope in situ hybridization using SIV-specific RNA probes was used to detect SIV-infected cells and cell-free virus in the spleens of TypP (**A**) and RP (**B**) infants. SIV+ cells were quantified across stitched images and normalized for area of splenic tissue (**C**). Statistical tests used to compare infant groups were carried out as described in the methods * = $p<0.05$. Error bars are shown as floating bars (min to max) with line indicating the mean. n = 3 per group.

Figure 10: Model summarizing factors influencing rapid SIV progression in infants Illustration of events following infection in infant macaques exhibiting rapid disease progression. GC = germinal center; Tfh = T follicular helper cell; pDC = plasmacytoid dendritic cell.

Table S1: Study Animals

Figure S1: Viral variants from RP infants are represented across more diverse challenge stock lineages. Phylogeny of macaque-derived plasma V1V2 variants isolated at 2 weeks post-infection(colored) and variants within challenge stock (black) (**A**). The number of clades in which each macaque-derived variant was represented was enumerated and the numbers of representative clades were compared between variants from TypP and RP macaques (**B**). Phylogenies were constructed using maximum likelihood with a GTR substitution model using the challenge stock consensus sequence. Statistical tests used to compare infant groups were carried out as described in the methods * = $p<0.05$. Error bars are shown as either mean with standard deviation or median with interquartile range based on data distribution.

Figure S2: Similar innate responses to microbial products are observed in typical and rapidly progressing infant macaques. Plasma sCD14(**A**) and LBP(**B**) concentrations were measured by ELISA at timepoints prior to and following SIV infection in TypP and RP infants. Statistical tests used to compare infant groups were carried out as described in the methods * = $p<0.05$

Figure S3: No differences are observed in levels of Resting Memory B cells, Tissue-Like Memory B cells, or IL-21R+ Activated Memory B cells in RP and TypP infants. Proportions of memory B cell subsets in TypP infants (**closed circles**) and RP infants (**open squares**). Percentages of resting memory B cells (RestMem, CD21+, CD27+) and Tissue-Like memory B cells (TLMem, CD21-,CD27-) were evaluated within the total B cell (CD20+) population in PMBC (**A+B**). The percentage of Activated Memory B cells (ActMem, CD21-, CD27+) was measured expressing the IL21 receptor (IL-21R) (**C**). Statistical tests used to compare infant

826 groups were carried out as described in the methods. Error bars are shown as either mean with
827 standard deviation or median with interquartile range based on data distribution.
828
829
830 **Footnotes**
831 The authors have no conflicts of interest to report.
832
833 This work was supported in part by the following National Institutes of Health awards: NIDCR
834 grant R01-DE023047. This work was also supported by the University of Washington
835 Pathobiology Training Grant T32-A1750915. The Washington National Primate Center is
836 supported by grant P51 OD010425 from the NIH Office of Research Infrastructure
837 Programs.
838 Corresponding author:
839 Donald Sodora
840 Seattle Children's Research Institute, Center for Global Infectious Diseases
841 Seattle, WA 98109
842 donald.sodora@seattlechildrens.org
843 Office: (206)884-3221
844

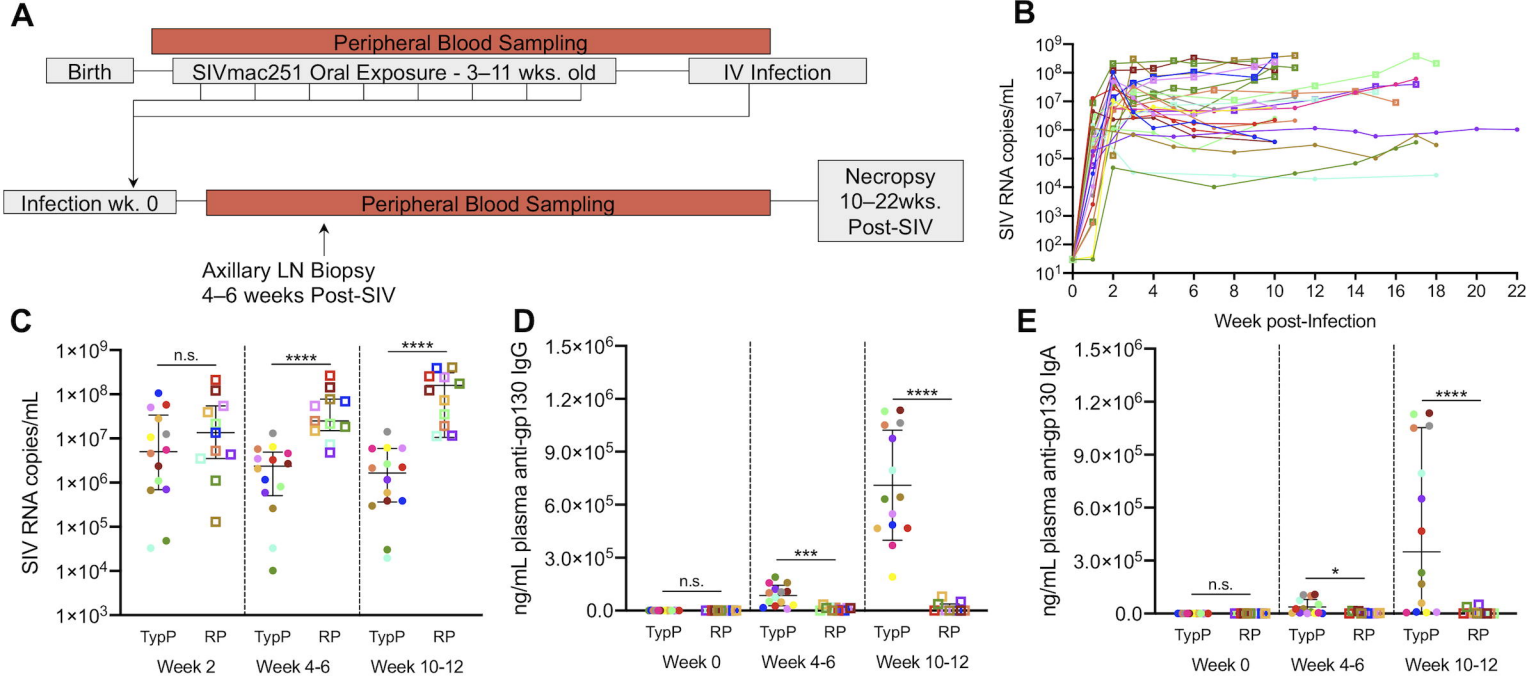
A
Peripheral Blood Sampling
Birth
SIVmac251 Oral Exposure - 3–11 wks. old
IV Infection
Infection wk. 0
Peripheral Blood Sampling
Necropsy
10–22wks.
Post-SIV
Axillary LN Biopsy
4–6 weeks Post-SIV
B
SIV RNA copies/mL
Week post-Infection
C
SIV RNA copies/mL
n.s.
****
****
TypP
RP
Week 2
Week 4-6
Week 10-12
D
ng/mL plasma anti-gp130 IgG
n.s.
***
****
Week 0
Week 4-6
Week 10-12
E
ng/mL plasma anti-gp130 IgA
n.s.
*
****
Week 0
Week 4-6
Week 10-12

Infant ID	Sex	MHC Class I Alleles	BCG Vaccinated	Disease Phenotype	Age SIV+ (wks)	Dose SIV+ (TCID50)	Viral Load at Necropsy
A14112-GD	M	A1*006, A1*006, B*012, B*048	Yes - Chronic SIV	TypP	14	10000	3.70E+05
A14113-GE	F	*A1*001*, A1*004, B*001, B*024	Yes - Chronic SIV	RP	14	10000	6.17E+07
A14114-GF	M	A1*004, A1*008, B*001, B*023	Yes - Chronic SIV	RP	18	4000	2.15E+08
A14115-GG	M	A1*008, A1*012, B*012, B*055	Yes - Chronic SIV	RP	14	10000	9.18E+06
A14203-HF	M	A1*002, A1*011, B*012, B*001	Yes - Chronic SIV	RP	8	4000	2.20E+07
A14206-HI	F	A1*004, A1*023, B*012, B*028	Yes - Chronic SIV	TypP	8	4000	3.01E+05
A15067-LA	F	–	Yes - 8 wks of age	RP	17	4000	1.04E+06
A15068-LB	F	–	Yes - 8 wks of age	TypP	17	4000	3.94E+07
A15187-MD	M	–	Yes - Chronic SIV	TypP	11	4000	2.65E+04
A16079-ZZ	F	A1*004, A1*023, B*001, B*012	No	RP	12	20000	2.43E+08
A16080-AA	F	A1*002, B*015	No	TypP	10	12000	6.03E+06
A16081-AB	F	A1*002, A1*006, B*012, B*024	No	RP	15	IV	3.91E+08
A16083-AD	M	A1*026, A1*002, B*001, B*055	No	TypP	11	15000	3.88E+05
A17151-FT	F	*A1*001*, A1*008, B*024, B*045	No	TypP	11	12000	2.14E+06
A17152-FU	F	A1*004, A1*011, B*001, B*066	No	RP	13	20000	4.04E+08
A17153-FV	F	A1*023, A1*025, **B*008**, B*028	No	TypP	6	1000	3.85E+05
A17154-FW	F	A1*002, A1*004, B*001	No	TypP	10	12000	1.41E+07
A16185-AT	F	A1*008, A1*032, B*012, B*068	Yes - 1-2 wks of age	TypP	10	12000	6.18E+06
A16187-AV	M	A1*002, *A1*001*, B*015, B*002	Yes - 1-2 wks of age	RP	8	4000	7.29E+07
A16188-AW	M	A1*004, B*012	Yes - 1-2 wks of age	RP	15	IV	2.55E+08
A16189-AX	M	A1*012, A1*025, **B*008**	Yes - 1-2 wks of age	TypP	15	IV	5.95E+05
A17097-FA	F	A1*008, A1*011, B*001, **B*008**	Yes - 1-2 wks of age	TypP	10	12000	2.23E+06
A17098-FB	M	A1*008, A1*023, B*012, B*015	Yes - 1-2 wks of age	RP	13	20000	1.51E+08
A17099-FC	F	A1*011, A1*023, B*012, B*024	Yes - 1-2 wks of age	RP	10	12000	1.22E+08
A17100-FD	M	A1*001, A1*023, B*002, B*028	Yes - 1-2 wks of age	TypP	13	20000	2.63E+06

Table S1: Study Animals

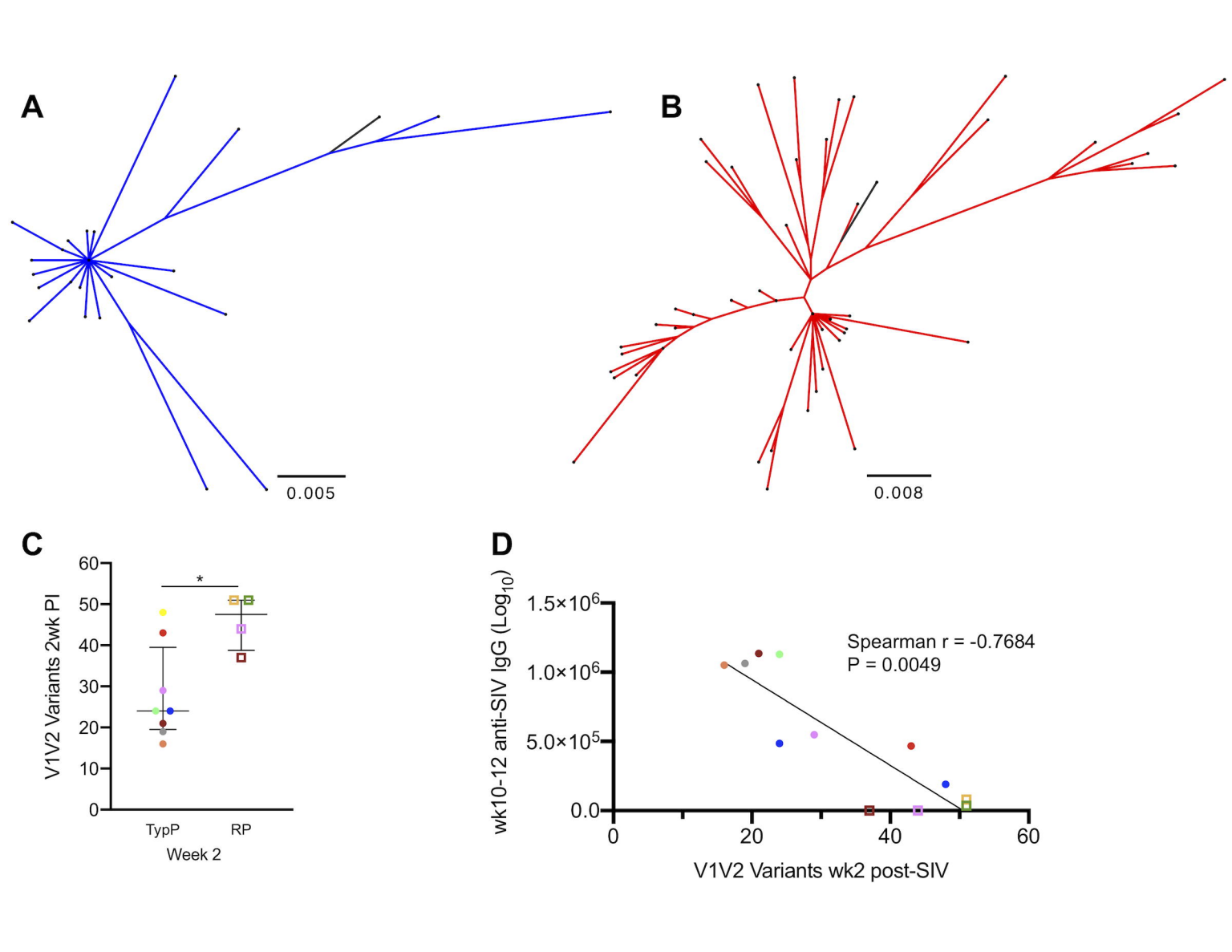
A
0.005
B
0.008
C
V1V2 Variants 2wk PI
60
50
40
30
20
10
0
*
TypP
RP
Week 2
D
wk10-12 anti-SIV IgG (Log10)
1.5×10^6
1.0×10^6
5.0×10^5
0.0
0
20
40
60
V1V2 Variants wk2 post-SIV
Spearman r = -0.7684
P = 0.0049

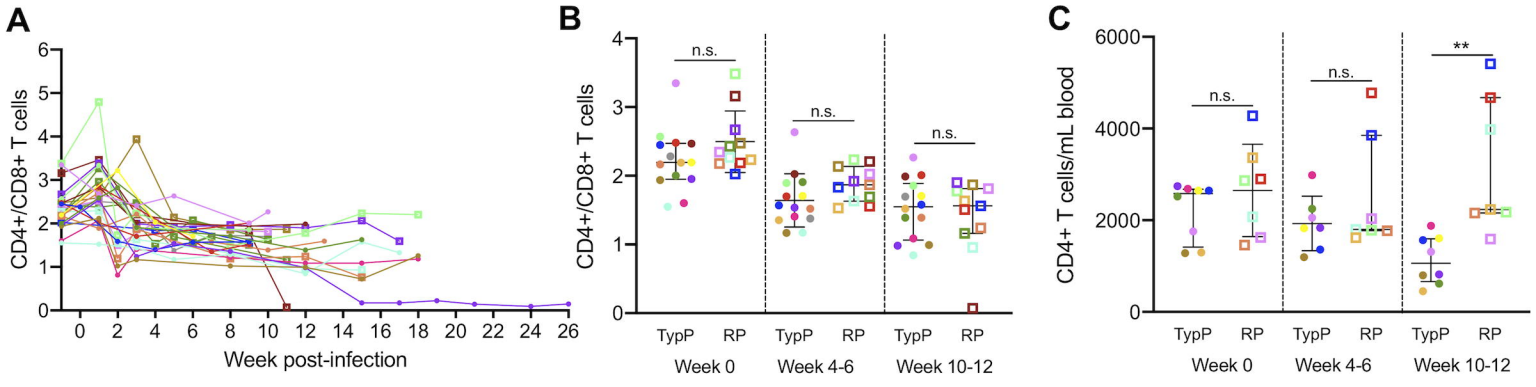
A
CD4+/CD8+ T cells
Week post-infection
B
CD4+/CD8+ T cells
n.s.
n.s.
n.s.
TypP
RP
Week 0
Week 4-6
Week 10-12
C
CD4+ T cells/mL blood
n.s.
n.s.
**
TypP
RP
Week 0
Week 4-6
Week 10-12

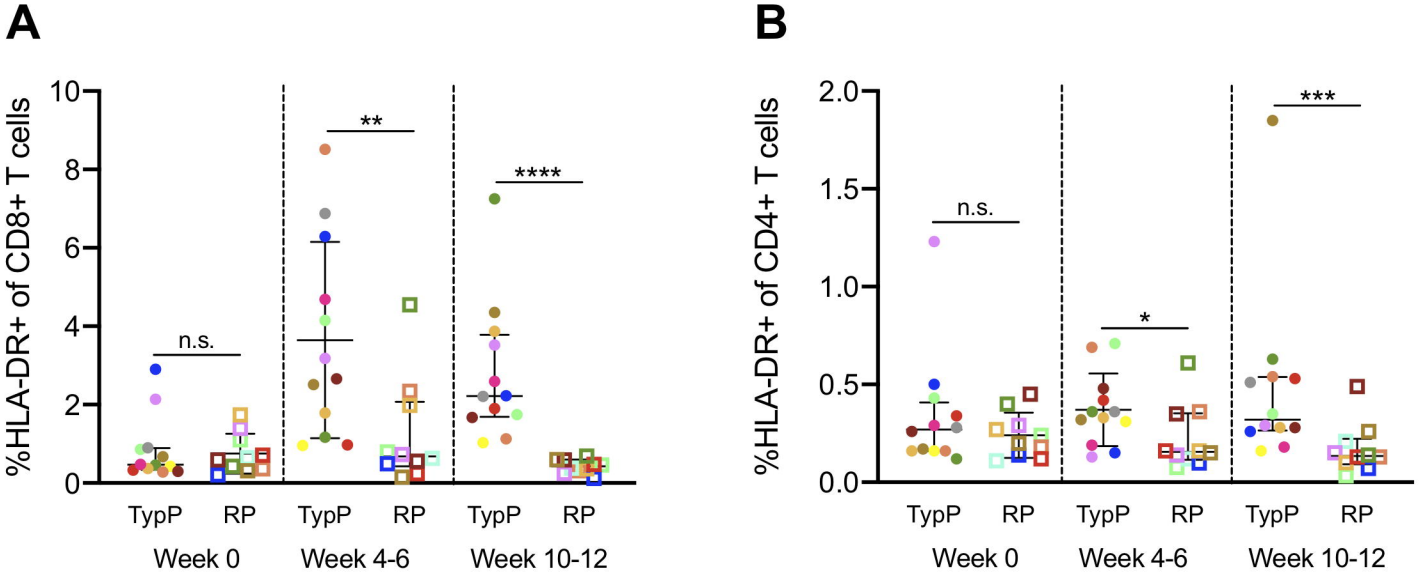
A
%HLA-DR+ of CD8+ T cells
10
8
6
4
2
0
n.s.
**
****
TypP
RP
TypP
RP
TypP
RP
Week 0
Week 4-6
Week 10-12
B
%HLA-DR+ of CD4+ T cells
2.0
1.5
1.0
0.5
0.0
n.s.
*
***
TypP
RP
TypP
RP
TypP
RP
Week 0
Week 4-6
Week 10-12

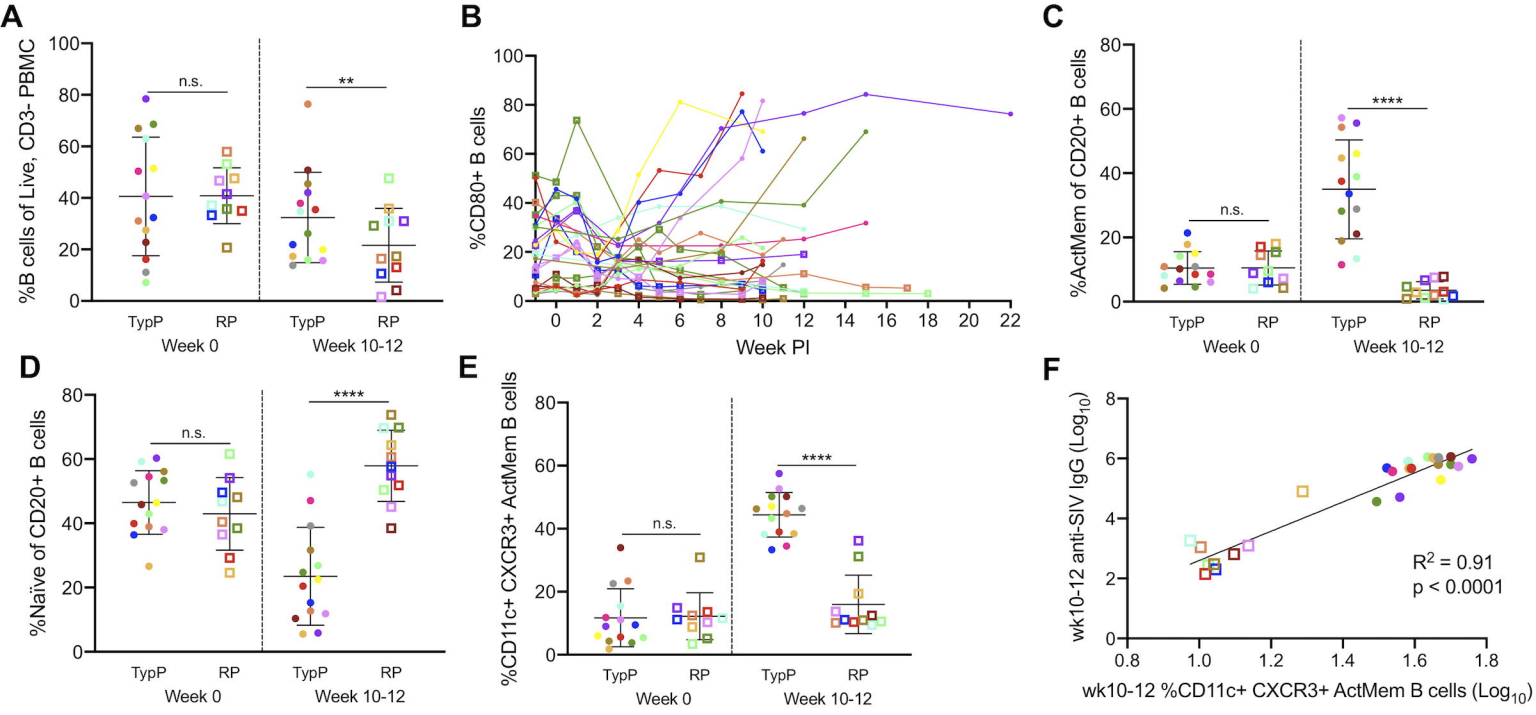
A
%B cells of Live, CD3- PBMC
n.s.
**
TypP
RP
TypP
RP
Week 0
Week 10-12
B
%CD80+ B cells
Week PI
C
%ActMem of CD20+ B cells
n.s.
****
TypP
RP
TypP
RP
Week 0
Week 10-12
D
%Naive of CD20+ B cells
n.s.
****
TypP
RP
TypP
RP
Week 0
Week 10-12
E
%CD11c+ CXCR3+ ActMem B cells
n.s.
****
TypP
RP
TypP
RP
Week 0
Week 10-12
F
wk10-12 anti-SIV IgG (Log10)
R2 = 0.91
p < 0.0001
wk10-12 %CD11c+ CXCR3+ ActMem B cells (Log10)

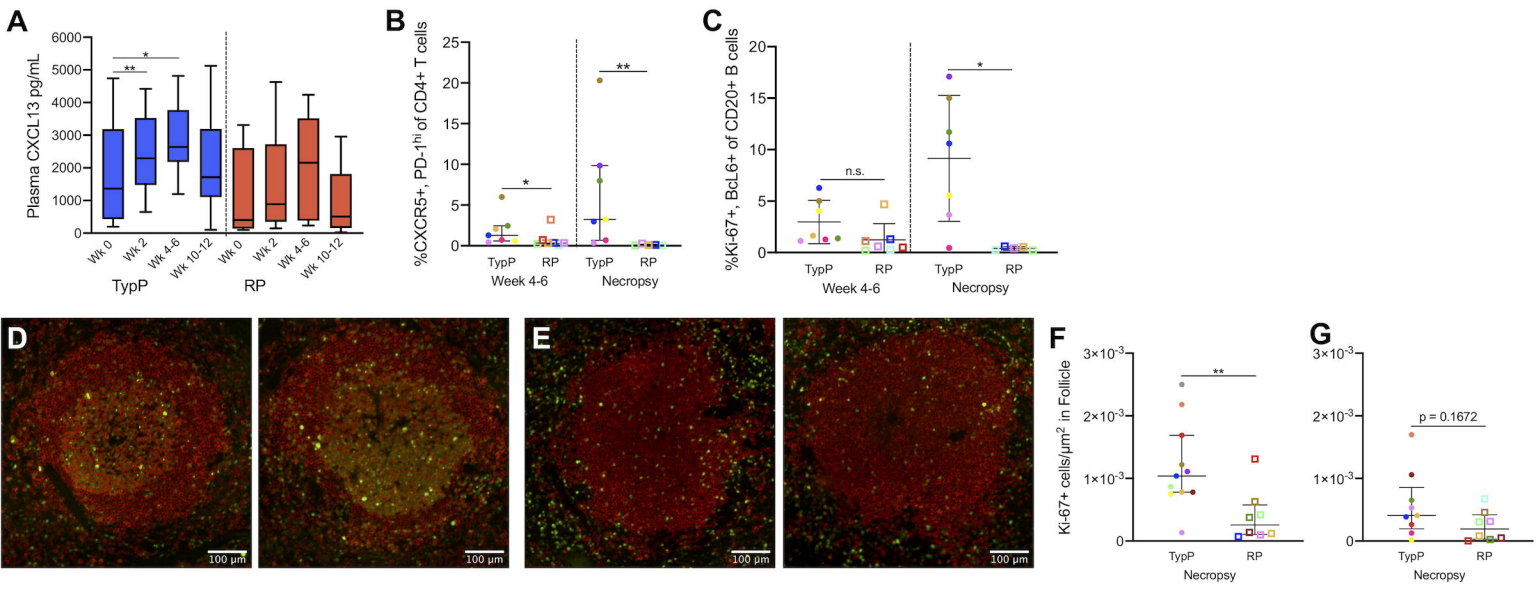
A
Plasma CXCL13 pg/mL
6000
5000
4000
3000
2000
1000
0
*
**
Wk 0
Wk 2
Wk 4-6
Wk 10-12
Wk 0
Wk 2
Wk 4-6
Wk 10-12
TypP
RP
B
%CXCR5+, PD-1hi of CD4+ T cells
25
20
15
10
5
0
*
**
TypP
RP
TypP
RP
Week 4-6
Necropsy
C
%Ki-67+, BcL6+ of CD20+ B cells
20
15
10
5
0
n.s.
*
TypP
RP
TypP
RP
Week 4-6
Necropsy
D
100 µm
100 µm
E
100 µm
100 µm
F
Ki-67+ cells/µm2 in Follicle
3×10-3
2×10-3
1×10-3
0
**
TypP
RP
Necropsy
G
3×10-3
2×10-3
1×10-3
0
p = 0.1672
TypP
RP
Necropsy

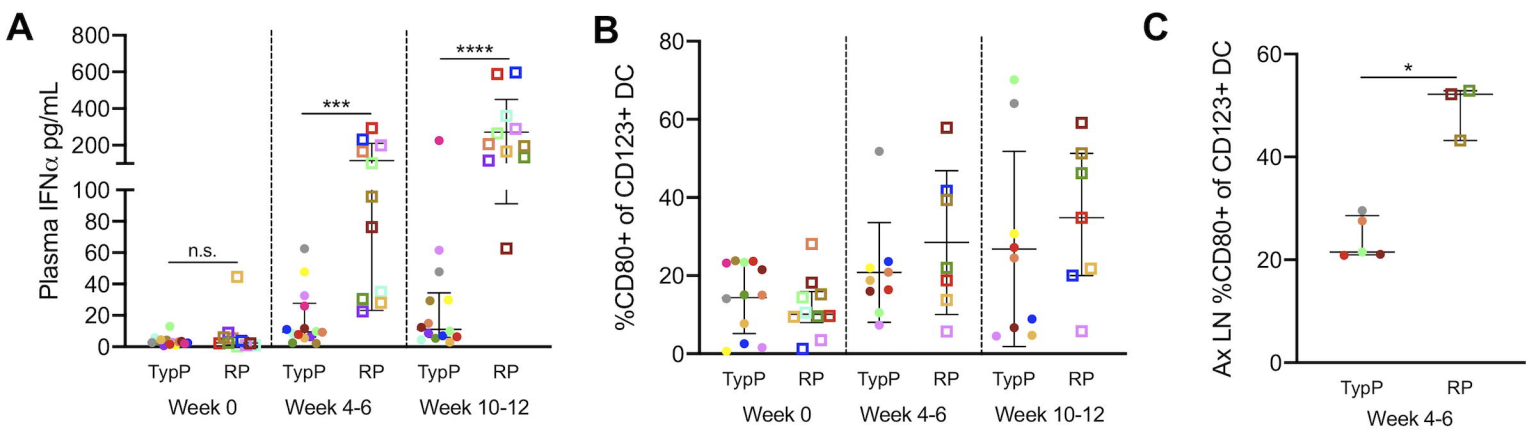
A
Plasma IFNα pg/mL
800
600
400
200
100
80
60
40
20
0
n.s.
***
****
TypP
RP
TypP
RP
TypP
RP
Week 0
Week 4-6
Week 10-12
B
%CD80+ of CD123+ DC
80
60
40
20
0
TypP
RP
TypP
RP
TypP
RP
Week 0
Week 4-6
Week 10-12
C
Ax LN %CD80+ of CD123+ DC
60
40
20
0
*
TypP
RP
Week 4-6

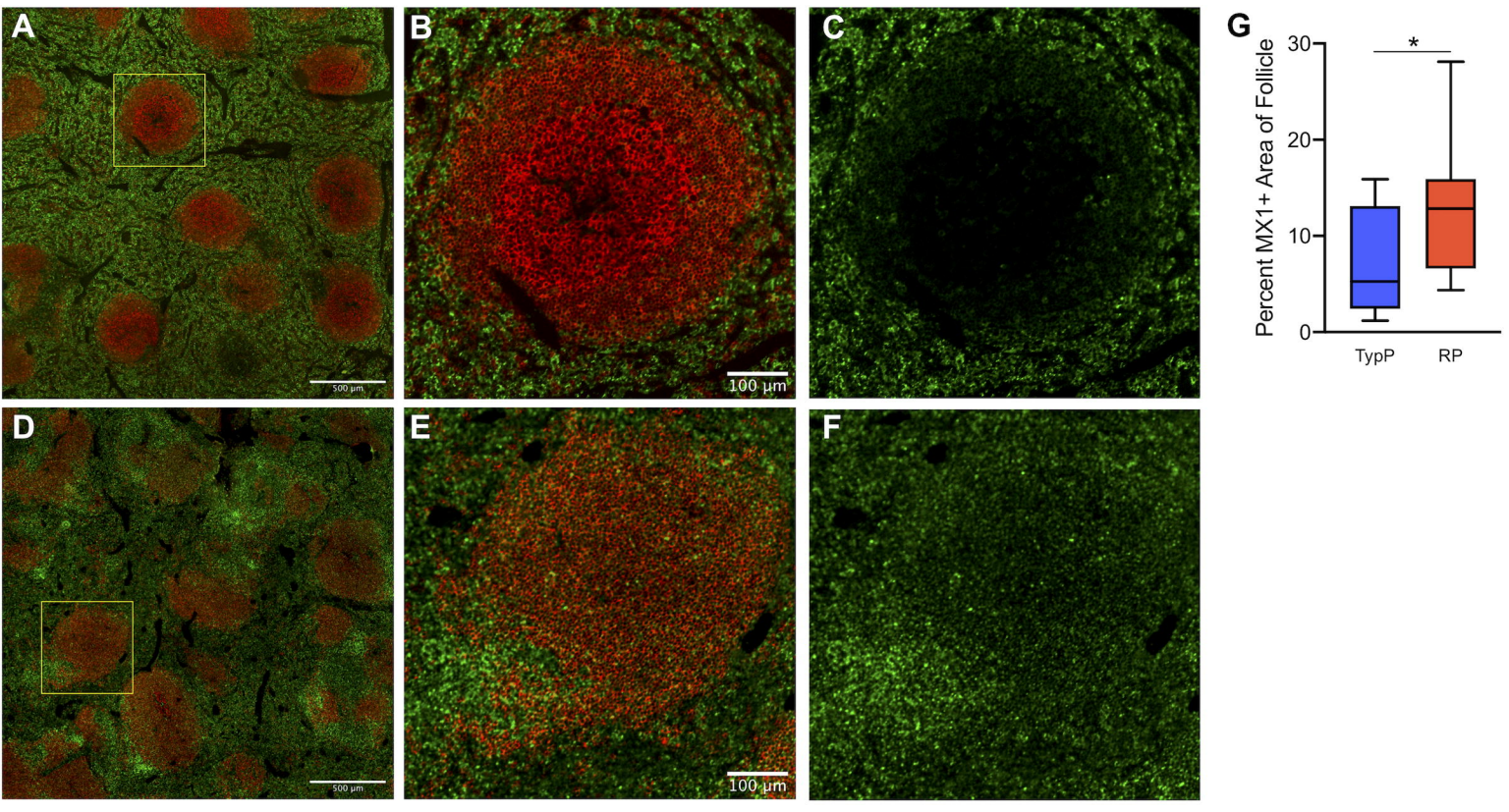
A
B
C
D
E
F
500 µm
100 µm
500 µm
100 µm
G
Percent MX1+ Area of Follicle
30
20
10
0
*
TypP
RP

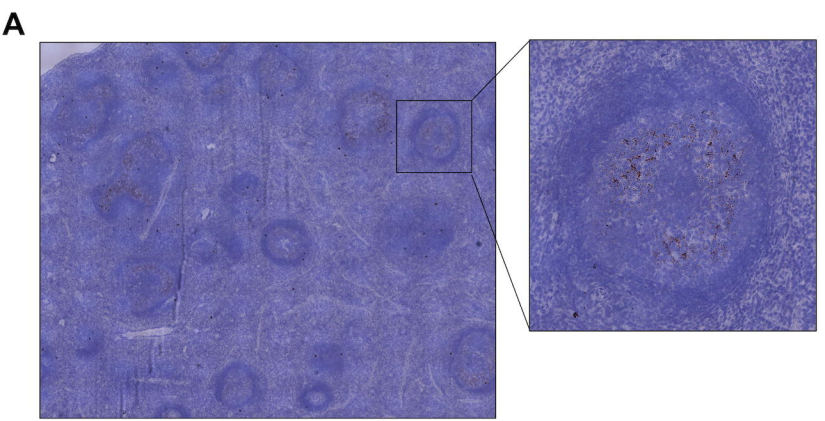
A

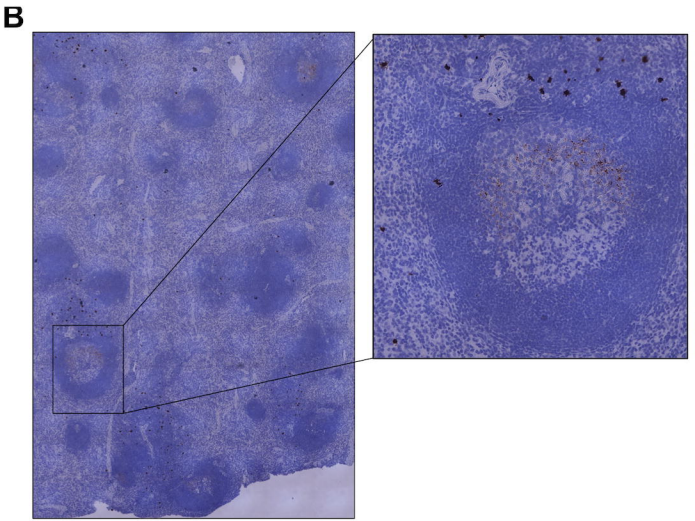
B

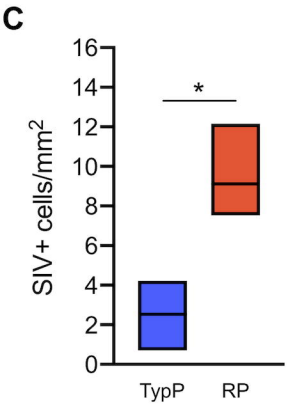
C
16
14
12
10
8
6
4
2
0
SIV+ cells/mm2
*
TypP
RP

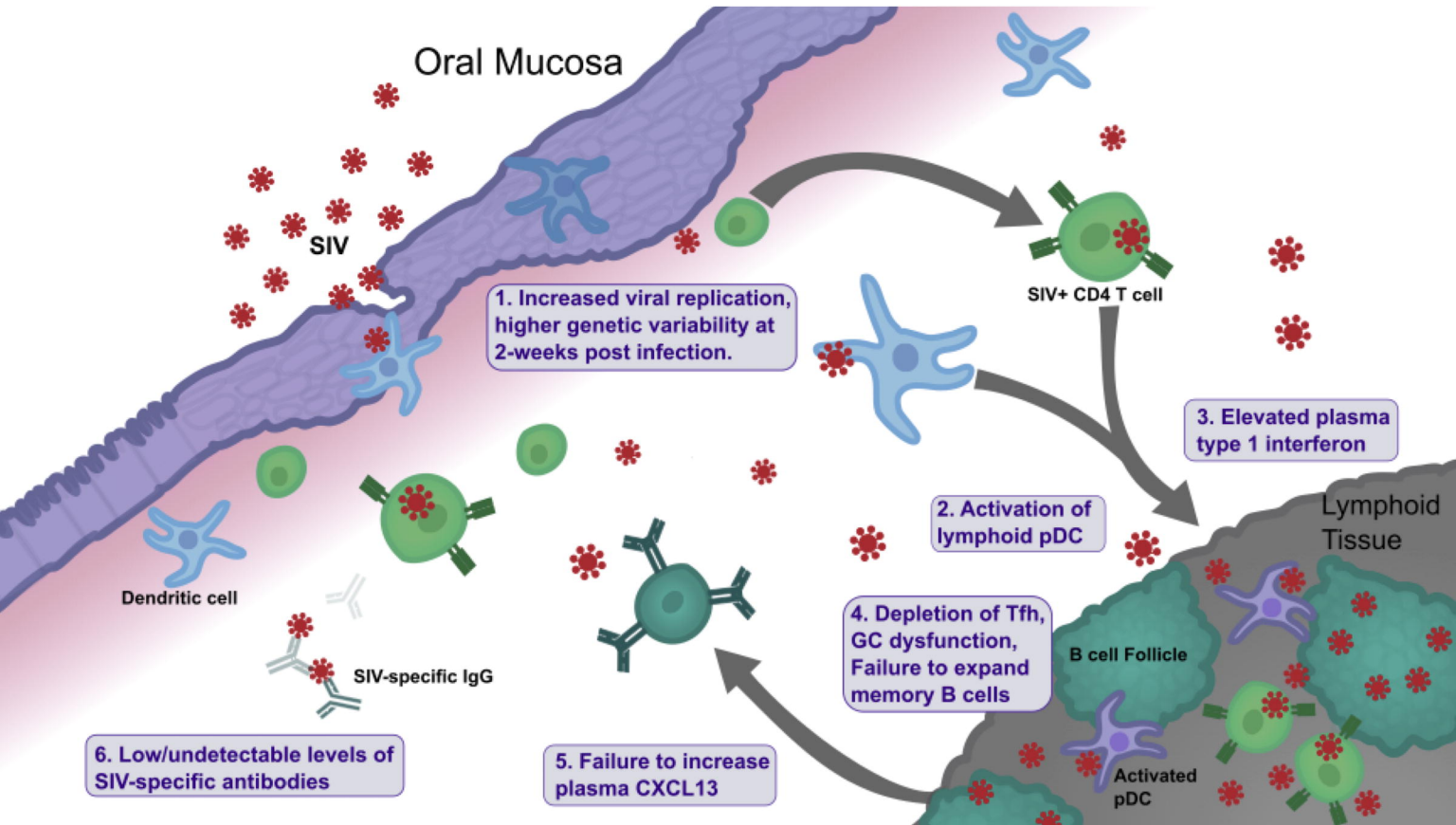
Oral Mucosa
SIV
1. Increased viral replication, higher genetic variability at 2-weeks post infection.
SIV+ CD4 T cell
3. Elevated plasma type 1 interferon
2. Activation of lymphoid pDC
Lymphoid Tissue
Dendritic cell
SIV-specific IgG
4. Depletion of Tfh, GC dysfunction, Failure to expand memory B cells
B cell Follicle
Activated pDC
5. Failure to increase plasma CXCL13
6. Low/undetectable levels of SIV-specific antibodies